The Astrophysical Journal, 698:1273–1281, 2009 June 20 doi:10.1088/0004-637X/698/2/1273

DETECTION OF FAR-INFRARED AND POLYCYCLIC AROMATIC HYDROCARBON EMISSION FROM THE COSMIC EYE: PROBING THE DUST AND STAR FORMATION OF LYMAN BREAK GALAXIES

B. Siana[1], Ian Smail[2], A. M. Swinbank[2], J. Richard[2], H. I. Teplitz[3], K. E. K. Coppin[2], R. S. Ellis[1], D. P. Stark[4], J.-P. Kneib[5], and A. C. Edge[2]

[1] California Institute of Technology, MS 105-24, Pasadena, CA 91125, USA
[2] Institute for Computational Cosmology, Durham University, South Road, Durham DH1 3LE, UK
[3] Spitzer Science Center, California Institute of Technology, 220-6, Pasadena, CA 91125, USA
[4] Institute of Astronomy, University of Cambridge, Madingley Road, Cambridge CB3 0HA, UK
[5] Laboratoire d'Astrophysique de Marseille, Traverse du Siphon, B.P. 8, F-13376 Marseille Cede 12, France
Received 2009 February 19; accepted 2009 April 13; published 2009 May 28

ABSTRACT

We report the results of a *Spitzer* infrared (IR) study of the Cosmic Eye, a strongly lensed, $L^*_{\rm UV}$ Lyman break galaxy (LBG) at $z = 3.074$. We obtained *Spitzer* mid-IR spectroscopy as well as MIPS 24 and 70 μm photometry. The Eye is detected with high significance at both 24 and 70 μm and, when including a flux limit at 3.5 mm, we estimate an IR luminosity of $L_{\rm IR} = 8.3^{+4.7}_{-4.4} \times 10^{11}\ L_\odot$ assuming a magnification of 28 ± 3. This $L_{\rm IR}$ is eight times lower than that predicted from the rest-frame ultraviolet properties assuming a Calzetti reddening law. This has also been observed in other young LBGs, and indicates that the dust reddening law may be steeper in these galaxies. The mid-IR spectrum shows strong polycyclic aromatic hydrocarbon (PAH) emission at 6.2 and 7.7 μm, with equivalent widths near the maximum values observed in star-forming galaxies at any redshift. The $L_{\rm PAH}$-to-$L_{\rm IR}$ ratio lies close to the relation measured in local starbursts. Therefore, $L_{\rm PAH}$ or $L_{\rm MIR}$ may be used to estimate $L_{\rm IR}$, and thus star formation rate, of LBGs, whose fluxes at longer wavelengths are typically below current confusion limits. We also report the highest redshift detection of the 3.3 μm PAH emission feature. The PAH ratio, $L_{6.2}/L_{3.3} = 5.1 \pm 2.7$, and the PAH-to-$L_{\rm IR}$ ratio, $L_{3.3}/L_{\rm IR} = 8.5 \pm 4.7 \times 10^{-4}$, are both in agreement with measurements in local starbursts and ultraluminous infrared galaxies (ULIRGs), suggesting that this line may serve as a good proxy for $L_{\rm PAH}$ or $L_{\rm IR}$ at $z > 3$ with the *James Webb Space Telescope*.

Key words: galaxies: high-redshift – galaxies: individual (J213512.73−010143, Cosmic Eye) – infrared: galaxies

1. INTRODUCTION

Star-forming galaxies at high redshift are often found by identifying a break in their ultraviolet (UV) continuum arising from both an intrinsic Lyman break in their spectral energy distributions (SEDs) and the high opacity of the Lyα forest below rest-frame 1216 Å (Steidel et al. 1996). Recent studies estimate that more than 25% of all present-day stellar mass was created in these Lyman break galaxies (LBGs) at $z > 2$ (Reddy & Steidel 2009). Their star formation rates (SFRs) typically have to be determined based on rest-frame UV properties alone. This involves using the UV spectral slope to determine the amount of UV extinction in order to derive the intrinsic UV luminosity and SFR. However, many uncertainties exist in this procedure. First, there are degeneracies between age and dust reddening on the UV spectral slope. Second, it is not clear that the obscuration law typically used to "unredden" the spectra is appropriate for LBGs. Furthermore, at least in the local universe, the most luminous starbursts contain individual star-forming regions that are so dusty that they effectively emit no UV light at all (Goldader et al. 2002), so the infrared (IR) and UV properties of these systems are uncorrelated.

Though it is more difficult to detect LBGs at other wavelengths, several studies have attempted to verify the UV-derived SFRs by comparing with other star formation diagnostics. With near-IR spectroscopy, Hα fluxes have been measured for >100 LBGs, and give comparable SFRs to the UV-derived SFRs (Erb et al. 2006). However, these Hα studies indicate that dust geometries may be different in LBGs than in local starbursts because the ionized gas does not seem to be more obscured than the stellar continuum, as is seen in local starbursts (Calzetti et al. 1994). X-ray stacking of large numbers of LBGs suggests comparable SFRs as the UV determinations (Reddy & Steidel 2004), but radio continuum stacking analyses have given mixed results (Reddy & Steidel 2004; Carilli et al. 2008). No individual detections of L^* LBGs (without active galactic nuclei (AGNs)) have been detected in the X-ray or radio.

Ultimately, the best indicator of the SFR is an accurate determination of the bolometric luminosity. Because most of the UV light (70%–90%) is absorbed by dust (Adelberger & Steidel 2000; Reddy et al. 2006), the majority of the starburst's luminosity is emitted thermally at IR wavelengths. With current technology, it is difficult to determine the IR luminosity as the SED cannot be measured at multiple wavelengths. Typical LBGs are below the confusion limit of existing submillimeter telescopes ($f_{850} < 2$ mJy; Chapman et al. 2000) and the *Spitzer Space Telescope* at 70 and 160 μm. *Spitzer* can only detect LBGs at 24 μm (rest-frame 6–8 μm) and then only $L > L^*$ LBGs are detected in the deepest images. Reddy et al. (2006) conducted a study of 24 μm detected LBGs (and stacks of nondetections) and concluded that that the average UV-derived SFRs are reliable. However, the MIPS 24 μm band only detects a few percent of the total IR luminosity and the bolometric corrections required to convert from the mid-IR flux to $L_{\rm IR}$ are large and highly uncertain, as the IR SEDs of LBGs have not been measured. Therefore, in addition to determining the validity of UV-derived SFRs, it would be useful to determine if the $L_{\rm MIR}$-to-$L_{\rm IR}$ conversions measured locally are valid in LBGs.

A few high-redshift LBGs have been found that are gravitationally lensed by foreground clusters or individual massive galaxies. Their high magnifications (factors of 10–30) mean that their IR fluxes are above the current far-IR confusion limits

and, in addition, mid-IR spectroscopy can be performed. These lensed LBGs can therefore be studied in the IR to better determine their SFRs and test whether star formation and dust extinction diagnostics measured in local starbursts are valid in LBGs.

The first detailed IR investigation of such a highly magnified LBG (MS1512-cB58) shows that the polycyclic aromatic hydrocarbon (PAH) strengths and the shape of the IR SED are similar to starbursts of comparable luminosity in the local universe (Siana et al. 2008). However, the IR luminosity is significantly lower than expected given the large dust extinction implied by cB58's red UV spectral slope, suggesting that the assumed dust extinction law (Calzetti et al. 2000) may not be valid for this galaxy. If this were true of other LBGs, it would suggest that the claimed estimates of their contribution to the SFR density in the early universe and, consequently, the time-integrated stellar mass density are too high. Of course, this is only one galaxy and there is quite a large dispersion measured in the UV–IR properties of local starbursts, so IR studies of more LBGs are required. Furthermore, cB58 is not a typical LBG in that it appears to be far younger than most LBGs ($t_{\rm age} < 30$ Myr), has a very red UV spectral slope, and displays stronger than average interstellar absorption lines.

Several other highly magnified LBGs have recently been found (Allam et al. 2007; Smail et al. 2007; Belokurov et al. 2007; Lin et al. 2008), with properties that span a broad range in parameter space occupied by LBGs (UV spectral slope, luminosity, inferred age, etc.). Detailed IR investigations of this entire sample can determine the UV/IR properties of typical high-redshift starbursts. In this paper, we report results of a *Spitzer* IR study of the Cosmic Eye (Smail et al. 2007) and compare with both the cB58 findings and relations measured in local starbursts.

The Cosmic Eye is an LBG at $z = 3.074$ (Smail et al. 2007) lensed by a massive foreground galaxy at $z = 0.73$, with a total magnification $\mu = 28 \pm 3$ (Dye et al. 2007). After modeling the foreground lens, reconstruction of the source image reveals the galaxy to be comprised of two UV components: a bright red and a fainter blue region. Like cB58, the combined component photometry shows a UV slope that is redder than typical LBGs (J. Richard et al. 2009, in preparation). Keck integral field spectroscopy has revealed that the two UV-luminous components are part of a well ordered, rotating disk (Stark et al. 2008). Detection of CO(3–2) emission indicates a large molecular gas reservoir ($\sim 2 \times 10^9\ M_\odot$) that is likely located in the fainter of the two UV components (Coppin et al. 2007).

We use a ΛCDM cosmology with $\Omega_m = 0.3$, $\Omega_\Lambda = 0.7$, and $H_0 = 70\ {\rm km\ s^{-1}\ Mpc^{-1}}$. All intrinsic luminosities and SFRs are corrected assuming a lensing magnification $\mu = 28 \pm 3$ (Dye et al. 2007).

2. OBSERVATIONS

Spitzer IRAC and MIPS 24 μm observations were taken as part of Director's Discretionary Time in 2006 November/December and are detailed in Coppin et al. (2007). Additional *Spitzer* observations using the InfraRed Spectrograph (IRS) and the Multiband Imaging Photometer for *Spitzer* (MIPS) were granted under Program ID 40817. IRS short-low first-order (7.4–14.5 μm) and long-low first-order (19.5–38.0 μm) observations were obtained on 2007 December 5. The spectra were taken in mapping mode, placing the galaxy at five different positions along the slits. The short-low (long-low) exposure times were 60 (120) s, with 50 (240) total exposures for a total of 3 (28.8) ks integration. The IRS data reduction was performed as specified in Teplitz et al. (2007). First, we removed latent charge by fitting the slope of the increase in background with time, and subtracting this background row by row. Second, "rogue" pixels were masked using the IRSCLEAN program provided by the *Spitzer* Science Center (SSC). Finally, the observations at other map positions were used to determine the sky, which was then subtracted. The individual frames were co-added to produce two-dimensional spectra at each map position. One-dimensional spectra were optimally extracted at each map position using the SPICE software provided by the SSC.

Table 1
Cosmic Eye Photometry

Band (μm)	Flux Density (μJy)	Error[a] (μJy)
16	90	18
24	281[b]	65[b]
70	4100	1300

Notes.
[a] Errors are 1σ.
[b] From Coppin et al. (2007).

The MIPS 70 μm observations were taken on 2007 November 28–29. 1080 exposures at nine dithered positions were taken for a total of 10.8 ks integration time. The MIPS 70 μm data were reduced using the Germanium Reprocessing Tools (GeRT), following the techniques optimized for deep photometry data given by Frayer et al. (2006). The images were then mosaiced with MOPEX (Makovoz & Khan 2005) and extracted with APEX (Makovoz & Marleau 2005).

The IRS Peak-Up Imaging (PUI) 16 μm observations were taken on 2007 December 6. 20 dithered exposures of 30 s were taken for a total of 600 s integration. A median sky was created and subtracted from each Basic Calibrated Data (BCD) frame. The BCDs were combined using MOPEX, using both temporal and spatial outlier rejections (Mosaic Outlier and Dual Outlier). Interpolation was performed using the drizzle algorithm with DRIZ_FRAC= 0.8 and an output pixel size of 0.″9 (half of the native PUI plate scale). We used APEX for source extraction, with a custom point-response function (PRF) made with the same drizzle parameters.

3. RESULTS

3.1. Infrared SED and L_{IR}

The 16, 24, and 70 μm photometry all yield greater than 5σ detections (see Table 1). We use these fluxes, combined with a 3.5 mm flux limit from Coppin et al. (2007) to fit the shape of the IR SED and determine the IR luminosity. The diameter of the Cosmic Eye is $\sim 2''$ and is therefore unresolved in any of the IRS and MIPS photometry (the 16, 24, and 70 μm point-spread function (PSF) FWHMs are $4''$, $6''$, and $18''$, respectively). Therefore, the foreground galaxy at $z = 0.73$ may be contaminating the mid-IR photometry. Here, we attempt to determine the magnitude of this foreground contamination.

In the optical spectrum obtained in Smail et al. (2007), the foreground galaxy has an [O II] 3727 Å emission line flux $f_{[\rm O\,II]} \sim 1.5 \times 10^{-17}$ erg s^{-1} cm^{-2}, or $L_{[\rm O\,II]} = 3.6 \times 10^{40}$ erg s^{-1}. Using the Kennicutt (1998) conversion to SFR, we get ${\rm SFR}_{fg}([{\rm O\,II}]) \sim 0.5\ M_\odot\ {\rm yr}^{-1}$. This assumes an extinction of $A_V = 1$. Converting this SFR to an $L_{\rm IR}$ using Kennicutt (1998),

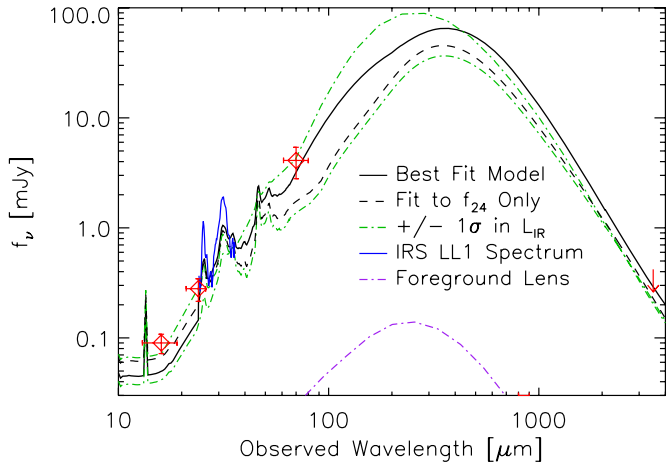

Figure 1. The observed IR SED of the Cosmic Eye. The best-fit SED from Chary & Elbaz (2001) to the 24, 70 μm, and 3.5 mm fluxes yields $L_{IR} = 8.3 \times 10^{11}\ L_\odot$. Also plotted is the SED derived from the 24 μm flux alone, the SEDs giving the $\pm 1\sigma$ deviations in L_{IR}, and the estimated IR SED of the foreground lens (based on the [O II] flux).

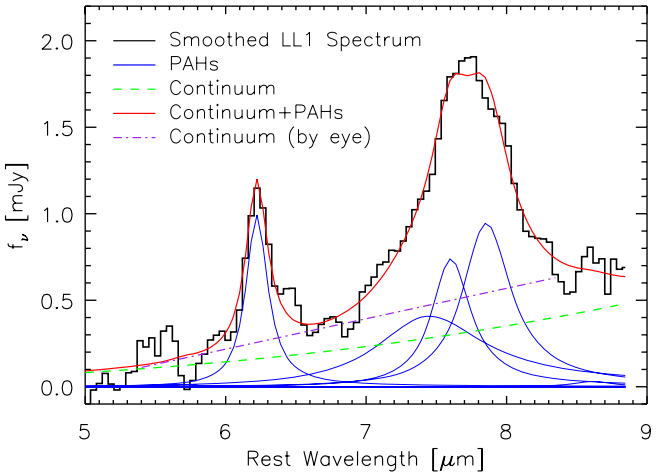

Figure 2. The smoothed IRS long-low spectrum of the Cosmic Eye. The simultaneous fit of the PAH features and continuum is also plotted. The dot-dashed line is the continuum assumed when computing PAH fluxes to compare with Pope et al. (2008).

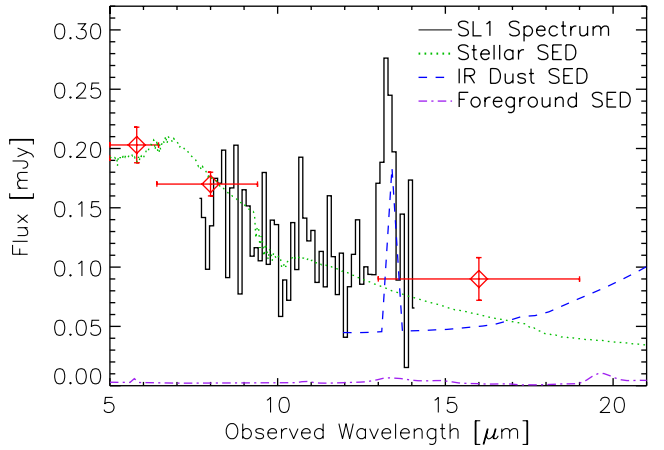

Figure 3. The IRS short-low spectrum of the Cosmic Eye. The feature at 13.3 μm is either 3.3 μm PAH emission at $z = 3.07$ or 7.7 μm PAH emission at $z = 0.73$. A stellar SED from a 100 Myr old (constant star formation) starburst is scaled to the IRAC bands. The SL spectrum was scaled up by 30% to match this SED. The best-fit Chary & Elbaz (2001) SED fit to the far-IR data is shown as well as a star-forming SED at $z = 0.73$ with an $L_{IR} = 2.3 \times 10^9\ L_\odot$ estimated from the foreground lens' [O II] emission line. The 3.3 μm PAH at $z = 3.074$ is expected to be much stronger than the 7.7 μm PAH at $z = 0.73$.

we get an $L_{IR} = 2.3 \times 10^9\ L_\odot$. If we choose an IR template typical of galaxies with this SFR (Chary & Elbaz 2001), the expected fluxes of the lens at 16, 24, and 70 μm are more than an order of magnitude lower than the observed fluxes (see Figure 1). Of course SFRs (and L_{IR}) based upon [O II] 3727 Å flux alone are quite uncertain due to unknown extinction and metallicity, but it seems very unlikely that the extinction is an order of magnitude higher than $A_V \sim 1$ in such an evolved massive galaxy.

As an additional check of foreground contamination, we also use the observed 16 μm flux to estimate the maximum IR contamination. The 16 μm band samples the minimum of the Cosmic Eye SED at $\lambda_{rest} = 4$ μm where both the stellar and dust SEDs are faint. However, the 16 μm band samples the possibly significant PAH emission from the foreground galaxy. By scaling the stellar SED to the IRAC bands, we find that the majority (>65%) of the measured $f(16\ \mu\text{m})$ is from the stars in the Cosmic Eye. This gives a conservative upper limit $f_{lens}(16\ \mu\text{m}) < 0.03$ mJy from the lens alone. This is in good agreement with the SED assumed when deriving the SFR in the lens from the [O II] 3727 Å flux. Therefore, estimates from both [O II] 3727 Å flux and the 16 μm flux show that the lens' contribution to flux at 24 and 70 μm is negligible.

Following the discussion above, we assume that the measured *Spitzer* fluxes are dominated by the Cosmic Eye. We fitted IR SED templates from Chary & Elbaz (2001) to the 24 and 70 μm photometry, as well as the 3.5 mm 1σ limit ($\lambda_{rest} \sim 870$ μm) from the CO observations ($f_{3.5\,mm} < 0.14$ mJy; Coppin et al. 2007). The best-fit template is a warm IR SED with a magnification corrected $L_{IR} = 8.3 \times 10^{11}\ L_\odot$ (see Figure 1). Other SED shapes are allowed that give a 1σ range of $L_{IR} = 3.9\text{–}13 \times 10^{11}\ L_\odot$. Using the conversion of Kennicutt (1998), we derive an $SFR_{IR} = 140 \pm 80\ M_\odot\ \text{yr}^{-1}$. If we select a template appropriate for the measured mid-IR luminosity, L_{MIR}, based on $f(24\ \mu\text{m})$ alone (as is often done at high redshift), we derive an IR luminosity nearly a factor of 2 smaller (see the dashed line in Figure 1, $L_{IR} = 4.8 \times 10^{11}\ L_\odot$). It is important to note that none of the templates gives an L_{IR} larger than $1.3 \times 10^{12}\ L_\odot$. This is because no cold or warm dust can be added without further violating the measurements at 3.5 mm or 70 μm, respectively. Because these fluxes may also have some foreground lens contamination, we take $L_{IR} < 1.3 \times 10^{12}\ L_\odot$ as a conservative upper limit.

3.2. Infrared Spectrum and PAH Luminosities

The IRS long-low spectrum is plotted in Figure 2. We see prominent PAH emission at rest-frame 6.2 and 7.7 μm. Unfortunately, the 8.6 μm feature lies close to the noisy end of the spectrum so its amplitude is uncertain. The PAH strengths were measured by simultaneously fitting Drude profiles with centers at the systemic redshift of the galaxy and widths defined by Draine & Li (2007), as well as a power-law continuum with a slope that is allowed to vary. The best-fit components are plotted in Figure 2 and the derived line fluxes are listed in Table 2. Some authors have determined PAH luminosities and equivalent widths (EWs) by simply assigning a continuum value based on the fluxes immediately longward and shortward of the features. Fluxes measured in this way are typically lower by up to a factor of 2. These fluxes are also listed in Table 2.

Table 2
Cosmic Eye Line Fluxes

Rest Wavelength (μm)	Observed Flux[a] (10^{-15} erg s^{-1} cm^2)	Luminosity[a,b] (10^{42} erg s^{-1})	Rest Equivalent Width (μm)
1.87 Paα	<0.41	<1.2	< 0.13
3.3 PAH	0.92 ± 0.17	2.7 ± 0.5	0.13
6.2 PAH	5.36 ± 1.23	15.7 ± 3.6	1.7
	(3.86)[c]	(11.3)[c]	(0.78)[c]
7.7 PAH	17.9 ± 4.48	52.4 ± 13.3	4.4
	(13.8)[c]	(40.3)[c]	(2.05)[c]
8.6 PAH	0.1 ± 2	0 ± 5	

Notes.
[a] Errors and limits are 1σ.
[b] Intrinsic luminosity after correction for assumed 28 × magnification.
[c] Values in parentheses are determined assuming the purple line in the figure as continuum 2 for continuum as in Pope et al. (2008).

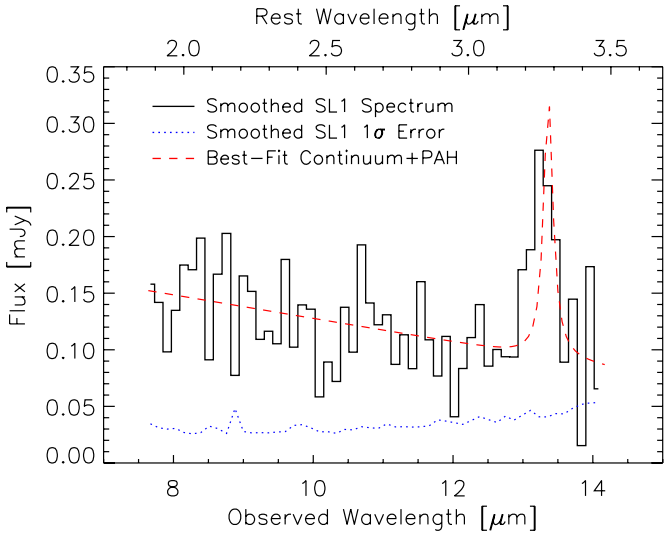

Figure 4. The short-low spectrum after binning by 2 pixels as well as the binned errors. The combined fit (to the unbinned data) of the 3.28 μm Drude profile and a linear continuum is also plotted. The 3.3 μm PAH feature is detected at 5.3σ.

The IRS short-low spectrum is plotted in Figure 3. The SL1 spectrum covers 7.5–14 μm and covers the Paα ($\lambda_{\rm rest}$ = 1.875 μm) and 3.3 μm PAH emission lines at $z = 3.074$. The Paα line is not seen but this is not surprising as an intrinsic SFR $\sim 140\ M_\odot\ {\rm yr}^{-1}$ gives an expected flux $f({\rm Pa}\alpha) = 2.3 \times 10^{42}$ erg s^{-1} (assuming a 28 × magnification) if the line is free of dust extinction. Therefore, we would only expect to detect it at less than 1.5σ. Here, we have assumed case B recombination and convert from the Hα-to-SFR conversion of Kennicutt (1998) using Pα/Hα = 0.128 (Hummer & Storey 1987).

An emission line is seen at $\lambda_{\rm obs} = 13.3$ μm. This can either be the 3.3 μm PAH feature at $z = 3.074$ or the 7.7 μm PAH line at the redshift of the foreground lens ($z = 0.73$). We believe that the feature is unlikely to be from the foreground lens. First, the flux falls off too quickly at $\lambda_{\rm obs} > 13.5$ μm, inconsistent with the broad 7.7 μm feature. Second, as seen in Figure 3, nearly all of the 16 μm flux can be explained by the stellar and dust emission from the Eye, without a significant contribution from PAHs from the foreground lens. So it is unlikely that the PAHs of the foreground lens are any stronger than the estimated foreground SED plotted in Figure 3 (see Section 3.1). In Figure 4, we show the binned (by 2 pixels) short-low spectrum with the best-fit (linear) continuum plus the 3.3 μm PAH profile and list the flux in Table 2. The 3.3 μm PAH feature is significant at 5.3σ.

4. DISCUSSION

The *Spitzer* data have confirmed strong PAH emission at 3.3, 6.2, and 7.7 μm. In addition, the 24 and 70 μm photometry in combination with the 3.5 mm flux limit give a good estimate of the shape of the IR SED and the $L_{\rm IR}$ (and the IR-derived SFR). In this section, we use these IR characteristics, as well as ancillary rest-frame UV and optical spectra, to compare with local star-forming galaxies of comparable luminosity as well as high-redshift, submillimeter-selected ultraluminous galaxies.

4.1. Infrared Excess versus UV Spectral Slope

We would like to determine whether the UV- and IR-derived SFRs agree if we assume the same relations measured in local starbursts. Typically, the UV spectral slope is used to determine the UV extinction, A_{1600}. The intrinsic UV luminosity can then be calculated and used to determine the UV-derived SFR, ${\rm SFR}_{\rm UV}$. We measure the UV spectral slope β (where $f_\lambda \propto \lambda^\beta$) in two ways: with broadband photometry and from the rest-frame UV spectrum itself. Broadband photometry mimics the method used for most LBGs, especially those that are fainter and/or at higher redshifts. It may seem better to derive the spectral slope directly from the spectrum, but the spectrum may suffer from differential atmospheric dispersion, only samples part of the total lens, and may have a small amount of contamination from the foreground lens (though this should be less than a few percent of the total flux). First, we use the high spatial resolution *Hubble Space Telescope* (*HST*) photometry of J. Richard et al. (2009, in preparation) and subtract a fit of the foreground lens profile. The resulting color, $V_{606} - I_{814} = 0.53 \pm 0.06$ (AB) gives an estimate of the spectral slope according to Equation (14) of Meurer et al. (1999). This equation takes into account the effect of interstellar absorption lines and the Lyα forest opacity below $\lambda_{\rm rest} < 1216$ Å (which affects a small fraction of the V_{606} band at this redshift). We also fitted the spectral slope to the parts of the optical spectrum that are uncontaminated by absorption lines. The spectrum is a composite of four parts of the entire ring (see Figure 1 of Smail et al. 2007), not the entire galaxy. Therefore, small differences in spectral slopes based on the photometry and spectra are expected. The best-fit slope from the spectrum, $\beta_{\rm spec} = 0.01$, is redder than the slope derived from the photometry alone, $\beta_{\rm photom} = -0.48$. We take the

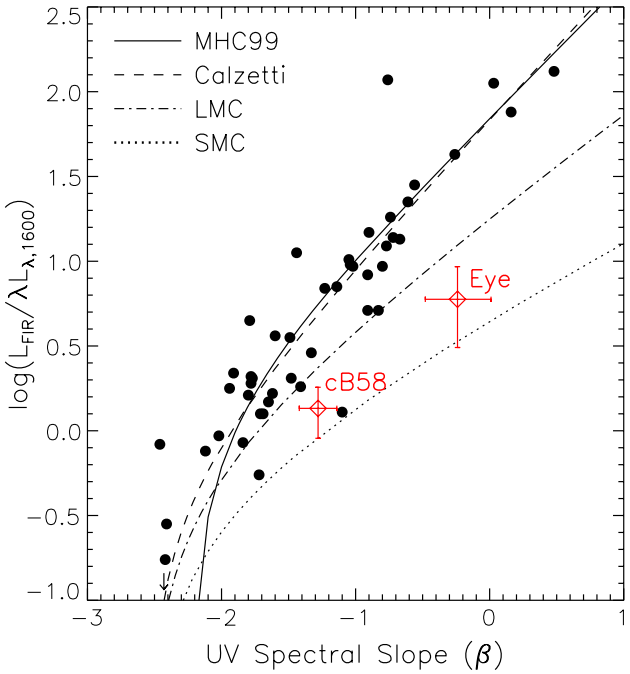

Figure 5. The far-IR (FIR; 40–120 μm) to UV (1600 Å) luminosity ratio vs. the UV spectral slope, β, defined as $f_\lambda \propto \lambda^\beta$. The best-fit relation of Meurer et al. (1999) and measurements of local starbursts are plotted. We show the expected IRX–β relation for three different reddening curves (Calzetti, LMC with out the 2175 Å feature, and SMC). The LMC and SMC extinction curves more accurately predict the observed FIR-to-UV ratios of the two lensed LBGs.

average of the two values and use the difference as the $\pm 1\sigma$ range. The resulting spectral slope, $\beta = -0.24 \pm 0.24$, is very red for LBGs, such that its observed optical colors lie near the edge of typical Lyman break color selection criteria.

Meurer et al. (1999) determined a relation between the UV spectral slope and the UV attenuation, A_{1600}. Essentially, this assumes that the starburst has an intrinsic spectral slope $\beta \sim -2.3$, and that the shape of the attenuation curve, A_λ, is that of the Calzetti reddening law (Calzetti 1997). The Meurer et al. (1999) relation suggests a UV attenuation, $A_{1600} = 3.95 \pm 0.74$ mag (the error here includes the 0.55 mag dispersion in the observed β-to-A_{1600} relation as well as the error in the spectral slope measurement). Correcting for this attenuation (and for the lens magnification), the measured UV luminosity is $L_{1500} = 6.3 \times 10^{30}$ erg s^{-1} Hz^{-1}. This translates to an SFR, $\mathrm{SFR_{UV}} = 900^{+900}_{-400}\ M_\odot\ \mathrm{yr}^{-1}$, using the conversion of Kennicutt (1998).

The UV-derived SFR is about six times that of the IR-derived SFR ($\mathrm{SFR_{IR}} = 140 \pm 80$) and even the 1σ lower limit is three times higher. The red UV spectrum suggests too much UV attenuation, which results in a predicted IR luminosity far above the maximum allowed L_{IR} from the observations. The same phenomenon was observed with the first lensed LBG to be studied in detail in the IR (cB58; Siana et al. 2008) as well as in *Spitzer* 24 μm studies of unlensed, young ($t_{\mathrm{age}} <$ 100 Myr) LBGs (Reddy et al. 2006). In Figure 5, we plot the far-IR to UV luminosity ratio versus UV spectral slope, β, fitted to a sample of local starburst galaxies (IRX–β; Meurer et al. 1999). This relation follows naturally assuming intrinsic spectral slopes typical of young starbursts ($-2.6 < \beta < -2.0$) and a Calzetti reddening law (Calzetti 1997). Because LBGs are assumed to have similar intrinsic spectral slopes as these local starbursts and are assumed to be reddened by something like a Calzetti law, this relation is generally used to infer IR luminosities and, thus, SFRs. In Figure 5, both cB58 and the Cosmic Eye lie below this relation by at least a factor of 4, beyond the typical scatter in this relation that is observed locally.

Of course, many local star-forming galaxies are known to lie off of this IRX–β relation. If much of the star-forming regions are completely extinguished in the UV, then the observed UV spectral slope will no longer be correlated with IRX. Goldader et al. (2002) showed this to be true in local ultraluminous infrared galaxies (ULIRGs) as they all lie above the IRX–β relation of Meurer et al. (1999).

If the intrinsic spectral slope is different due to different metallicities or star formation histories, this will cause galaxies to move significantly away from the measured relation. For example, less active star-forming galaxies such as nearby spirals are known to fall to the right of the IRX–β relation because their relatively large amount of less massive (older) stars makes the intrinsic spectral slope redder (Bell 2002).

Finally, if the reddening curve is significantly different than the assumed Calzetti reddening curve, this will affect the total amount of absorbed luminosity for a given UV spectral slope. For example, the SMC extinction curve (Prevot et al. 1984) is much steeper than the Calzetti law and can produce red UV slopes without extinguishing as much total luminosity as with a Calzetti law. Therefore, if the dust extinction in a particular galaxy follows an SMC curve, its IR luminosity would be far lower for a given β and would lie below the IRX–β relation.

Because these LBGs are so well characterized, we can investigate whether any of their known properties might explain why they lie below the relation observed in local starbursts. Using the R_{23} index (Pettini & Pagel 2004; Pilyugin & Thuan 2005), Stark et al. (2008) determine a metallicity for the Cosmic Eye of $\sim$0.9 $Z_\odot$. SED fits to the Cosmic Eye optical and near-IR photometry (J. Richard et al. 2009, in preparation) give ages of 80–300 Myr depending upon the exact star formation history. Both the metallicity and starburst age of the Cosmic Eye are similar to that of the local starburst sample and the estimated intrinsic UV spectral slope is $\beta \sim -2.4$, similar to the intrinsic slopes estimated for the local sample. cB58 has a metallicity of about $\frac{1}{3}$ $Z_\odot$ (Pettini et al. 2000; Teplitz et al. 2000) and a very young starburst age ($t_{\mathrm{age}} < 30$ Myr; Ellingson et al. 1996; Siana et al. 2008). The Bruzual (2007) models give an intrinsic slope of $\beta \sim -2.7$ for this metallicity and star formation history, bluer (more negative) than assumed for the local starbursts. Therefore, cB58 should lie to the *left* of the local relation, not to the right.

Given the intrinsic slopes predicted by their star formation histories and metallicities, both the Eye and cB58 should lie near (or to the left) of the local IRX–β relation if the Calzetti reddening law (Calzetti 1997) were valid in these LBGs. Therefore, we conclude that the reddening law in these two LBGs must be different than that measured in the local starburst sample. In Figure 5, we show three predicted IRX–β relations assuming different reddening curves: Calzetti, LMC (Fitzpatrick 1986) with no 2175 Å feature, and SMC. A reddening law that is steeper than the Calzetti curve, like the LMC or SMC, causes UV spectral slopes to become redder without extinguishing as much total UV luminosity. Thus, for the same observed UV spectral slope, the steeper reddening curves result in lower $L_{\mathrm{FIR}}/L_{\mathrm{UV}}$ than predicted by the Calzetti curve. As seen in Figure 5, both the Cosmic Eye and cB58 have $L_{\mathrm{FIR}}/L_{\mathrm{UV}}$ ratios indicative of steeper reddening laws.

Siana et al. (2008) conclude that the large covering fraction of outflowing, low-ionization gas (and presumably dust) seen in

the rest-frame UV spectrum of cB58 is indicative of a uniform foreground sheet of dust, rather than a patchy distribution that gives rise to a Calzetti curve. The rest-frame UV spectrum of the Cosmic Eye also exhibits opaque interstellar absorption lines indicating a similarly large covering fraction of outflowing gas. A uniform foreground sheet of dust results in reddening laws analogous to the LMC or SMC extinction curves (assuming similar dust compositions). As shown above, these steeper curves can explain why these LBGs fall below the local IRX–β relation. Therefore positions of the Cosmic Eye and cB58 on the IRX–β diagram can be explained if much of the dust obscuration is occurring in outflowing dust with a large covering fraction.

Alternatively, a different reddening curve could be caused by a different dust composition. It is possible that in a young galaxy with active star formation, a larger fraction of the dust is produced by core collapse supernovae (SNe) relative to dust produced by Type Ia SNe or evolved, low-mass (e.g., asymptotic giant branch (AGB)) stars. Evidence for extinction due to dust from Type II SNe (Todini & Ferrara 2001) has been observed in host galaxies of a QSO and a gamma-ray burst at $z \sim 6.2$–6.3 (Maiolino et al. 2004; Stratta et al. 2007), when the age of the universe is less than the time required for stars to evolve to the AGB phase (when much of the dust is deposited into the interstellar medium (ISM)). Because the star formation activity in these two LBGs is recent (<300 Myr), this could imply that the fraction of dust from Type II SNe to dust from AGB stars is larger in these systems, which may affect the shapes of the reddening curves. However, both LBGs show strong emission from PAHs, which are thought to be produced primarily in AGB stars (Latter 1991; Tielens 2008), so it is possible that there exists a population of less luminous, older stars that is also depositing dust into the ISM.

It is impossible to make any broad conclusions about the LBG population as a whole based on these two LBGs alone. However, it is instructive to note that at least a subset of LBGs may not obey the typical relations assumed for all LBGs. It appears that UV-derived SFRs of young LBGs with strong interstellar absorption features may be overestimated by a factor of ∼4–5. According to SED fits to the rest-frame UV–optical photometry, ∼20% of all $\sim L^*$ LBGs have starburst ages less than 100 Myr (Shapley et al. 2001; Papovich et al. 2001). Therefore, any large (factor ∼4) adjustment to their derived SFRs will significantly impact the total SFR density at high redshift.

Of course, many high-redshift galaxies also lie *above* the local relations such that their UV properties *under*predict their total SFRs (Reddy et al. 2006). However, many of these galaxies (e.g., submillimeter continuum selected galaxies) are accounted for separately when determining SFR densities at high redshift (Chapman et al. 2005).

4.1.1. Caveats

There are a few complications in our analysis that arise because we are observing a lensed galaxy. The first is that the UV-luminous portions of the Eye may lie closer to the caustic than the IR-luminous regions and are therefore more highly magnified, resulting in the source lying below the local IRX–β relation. This is especially relevant as the Eye was selected for its bright rest-frame UV fluxes, not its IR fluxes, so we may be biased toward galaxies with high UV magnifications. Source reconstruction of the Cosmic Eye shows that the most UV-luminous region lies near the caustic and is thus highly magnified (Dye et al. 2007). If the central region of the galaxy, which is further from the caustic (see Figure 2 in Stark et al. 2008), hosts a more obscured starburst (as is commonly observed in local LIRGs), this region will not be so highly magnified, and the observed $L_{\rm IR}$-to-$L_{\rm UV}$ ratio will not be the same as the ratio observed without the foreground lens.

Of course, for this phenomenon to bias our results, the small-scale star-forming regions within the LBGs must violate the local IRX–β relationship (i.e., the UV and IR fluxes are uncorrelated at subkpc scales). There is no evidence that this is the case in local galaxies. For example, individual star-forming regions in M51a appear to show similar trends at scales <500 pc (though the trend is offset due to the presence of older stellar populations; Calzetti et al. 2005). If we assume that the UV and IR emissions in LBGs are also correlated on scales smaller than 500 pc, then the effect of differential magnification on our results is mitigated significantly.

It is also possible that there is dust present around the foreground lens that is further reddening the UV spectrum of the background LBG. This would affect the observed UV spectral slope, but would not significantly increase the observed $L_{\rm IR}$. This would require significant columns of dust at large radii from the center of the foreground lensing galaxies (∼7 physical kpc for the lens of the Cosmic Eye). There are many galaxies with dust at >7 kpc. For example, Engelbracht et al. (2006) find emission from PAHs in SNe winds at >6 kpc from M82. The Sa galaxy, the Sombrero galaxy, and the Sd galaxy, NGC 4594, both have dust at radii of ∼7 kpc (Bendo et al. 2006a, 2006b). Also, recent *Galaxy Evolution Explorer* (*GALEX*) observations have found low levels of star formation (where some dust is presumably present) in the extreme outer disks of M83 and NGC 4625 (∼10 kpc; Thilker et al. 2005; Gil de Paz et al. 2005). However, these dust features and low level star-forming regions are found in large spiral disks (e.g., M83) or actively star-forming galaxies (M82), and are not typically found around massive ellipticals. Furthermore, when the dust is present, it is patchy and distributed along spiral arms and has low optical depths at the relevant wavelengths ($\tau(4000\ \text{Å}) < 0.3$; Holwerda et al. 2009). Given the high stellar mass and low SFR of the foreground lens of the Cosmic Eye and the fact that the color changes very little around the ring of the Eye, we expect the foreground extinction to be negligible.

4.2. PAH Properties

4.2.1. Mid-IR Spectra Comparison

In Figure 6, we compare the mid-IR spectra of the Cosmic Eye with another lensed LBG (cB58; Siana et al. 2008), a composite of high-redshift submillimeter-selected ULIRGs (Menéndez-Delmestre et al. 2009), and a composite of low-redshift, lower luminosity ($L_{\rm IR} < 10^{11}\ L_\odot$) starburst galaxies (Brandl et al. 2006). All of the spectra exhibit high PAH EWs and the PAH ratio, $L_{7.7}/L_{6.2}$, is approximately constant in all of these spectra except for the SMG composite, which has a markedly higher ratio than the others. This PAH ratio does not change with ionization state of the PAHs, but changes dramatically with grain size distribution (Draine & Li 2007). The discrepancy may suggest that grain sizes are relatively larger in SMGs than in LBGs and local starbursts. However, there is significant dispersion in all of the populations so a comparison of one or two LBGs to the SMG sample as a whole is not definitive.

Because the 7.7 μm feature is confused with the 8.6 μm feature and the broad silicate absorption at 9.7 μm, we choose to use the 6.2 μm PAH EW for comparison with other works. In

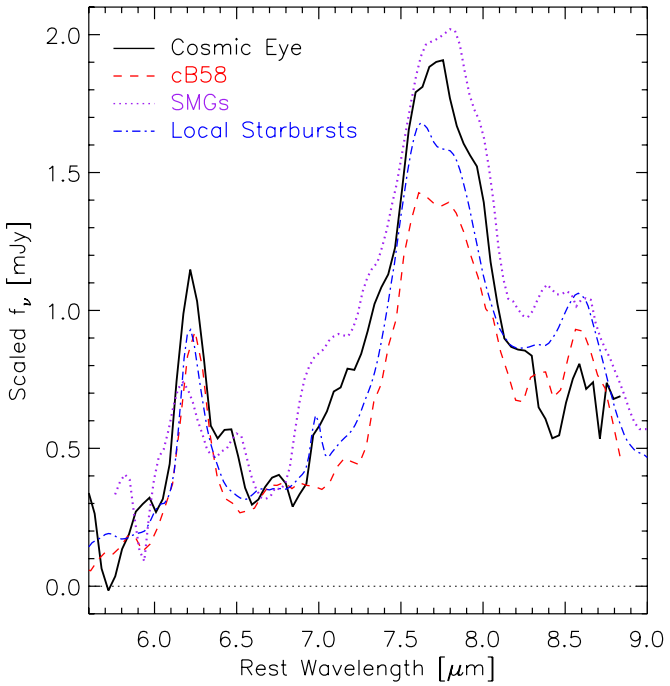

Figure 6. Comparison of mid-IR spectra (normalized to the 6.7 μm continuum) of the Cosmic Eye, cB58 (Siana et al. 2008), an SMG composite (Menéndez-Delmestre et al. 2009), and a local starburst composite (Brandl et al. 2006). These galaxies span 3 orders of magnitude in luminosity in $L_{\rm IR}$ (10^{10}–10^{13} $L_\odot$). The mid-IR spectra of the LBGs (Cosmic Eye and cB58) and the local starburst composite are similar. However, the $L_{7.7}/L_{6.2}$ ratio of the SMGs is markedly higher than in the LBGs or local starbursts.

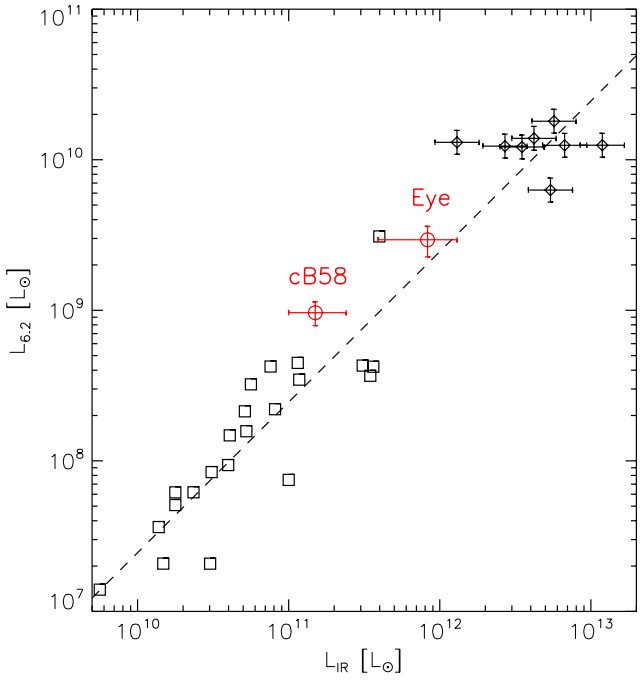

Figure 7. The 6.2 μm PAH strength vs. IR luminosity. This figure is adapted from the top panel of Figure 12 in Pope et al. (2008). Local starbursts (squares) are from Brandl et al. (2006) and high-redshift SMG (diamonds) are from Pope et al. (2008). The dashed line is the best-fit $L_{6.2}$-to-$L_{\rm IR}$ relation of Pope et al. (2008) for the low-redshift starbursts. The $L_{\rm PAH}/L_{\rm IR}$ ratios of the two lensed LBGs are consistent with the extrapolation (to higher luminosities) of the trend observed in local starbursts.

Table 2, we list the derived rest-frame EWs of the PAHs using two separate methods: by simply defining a linear continuum on either side of the PAHs and by simultaneously fitting all PAHs and a power-law continuum. The other studies to which we are comparing have derived EWs in a manner similar to the former method. Therefore, we use the EWs listed in parentheses in Table 2 for comparison. The rest-frame EW, $\rm EW_{6.2} = 0.78$ μm, is very high, near the maximum values found in local star-forming galaxies with no AGN activity (Brandl et al. 2006; Desai et al. 2007; Imanishi et al. 2007) as well as high-redshift ULIRGs with strong PAH emission (Sajina et al. 2007; Pope et al. 2008).

4.2.2. L_{PAH} *versus* L_{IR}

In Figure 7, we plot the 6.2 μm PAH luminosity versus $L_{\rm IR}$ for the Eye relative to local starbursts (Brandl et al. 2006), high-redshift SMGs (Pope et al. 2008), and cB58 (Siana et al. 2008). We have remeasured our PAH luminosities in a similar manner as that of Pope et al. (2008) by selecting the continuum level on either side of the PAH features, rather than simultaneously fitting all features and the continuum. These PAH luminosities are also listed in Table 2. Both cB58 and the Cosmic Eye lie above the measured relation of Pope et al. (2008) but certainly within the rather large scatter. Therefore, for these two LBGs, it appears that the 24 μm flux, which is dominated by PAH emission, would give a reasonable estimate of the $L_{\rm IR}$, lending credence to high-redshift ($1.5 < z < 3.0$) SFR determinations based on *Spitzer* 24 μm fluxes alone. A similar study of lensed galaxies of somewhat higher IR luminosities at high redshift has also found that rest-frame 8 μm fluxes also reproduces the $L_{\rm IR}$ reasonably well (Rigby et al. 2008).

4.2.3. 3.3 μm PAH

We have a 5σ detection of the 3.3 μm PAH feature. This is the highest redshift galaxy in which this feature has been detected, and only the second (the first was reported in Sajina et al. 2009) to be detected outside of the local ($z < 0.2$) universe (Moorwood 1986; Imanishi & Dudley 2000; Imanishi et al. 2006; Risaliti et al. 2006). The 3.3 μm PAH feature will be particularly useful in future studies of dust and star formation as it is the only PAH emission feature accessible to the *James Webb Space Telescope* (*JWST*) at $z > 3$. Therefore, it is important to characterize how well $L_{3.3}$ scales with other PAHs and $L_{\rm IR}$ in LBGs at $z < 3$ so that *JWST* studies can properly interpret measurements at higher redshift. The PAH ratio, $L_{6.2}/L_{3.3} = 5.8 \pm 1.7$, is consistent with the typical ratio measured in local ULIRGs ($\langle L_{6.2}/L_{3.3}\rangle = 5.6$; Imanishi et al. 2006, 2007). Here, we have used only isolated and compact galaxies in Imanishi et al. (2006, 2007), to minimize the effects due to different slit widths between the L band and *Spitzer* slits, though Imanishi et al. (2008) compare their L-band spectra with Akari slitless spectra and find no evidence for significant slit loss. The $L_{3.3}/L_{\rm IR} \sim 8.5 \pm 4.7 \times 10^{-4}$ ratio (or $L_{3.3}/L_{\rm FIR} \sim 1.5 \times 10^{-3}$ when using far-IR rather than total IR luminosity) is consistent with the ratio measured in local starburst galaxies ($L_{3.3}/L_{\rm FIR} \sim 1 \times 10^{-3}$; Mouri et al. 1990; Imanishi 2002), suggesting that this PAH feature may be used as an indicator of $L_{\rm IR}$ at high redshift. We note that the measured $L_{3.3}/L_{\rm IR}$ is about five times lower than the ratio inferred from a recent broadband (*Spitzer* IRAC) estimate of the 3.3 μm feature in LIRGs at $z \sim 0.7$ (Magnelli et al. 2008).

5. CONCLUSIONS

Due to the strong magnification (factor of $\sim$28$\times$) of the Cosmic Eye, we are able to perform a *Spitzer* IR study of

an otherwise inaccessible L^*_{UV} LBG. We obtain high signal-to-noise ratio (S/N) ($>5\sigma$) detections at 16, 24, and 70 μm, as well as high S/N IRS short-low and long-low spectra from 7.4–14.5 μm and 19.5–35 μm, respectively. With these data we compare different star formation diagnostics, and compare the IR properties to other star-forming galaxies at low and high redshift. We find the following:

1. Using the [O II] and maximum 16 μm fluxes of the foreground lens, we argue that far-IR photometry and mid-IR spectroscopy of the Cosmic Eye are not significantly contaminated by the lens.
2. The IR photometry of the Eye (including a 3.5 mm flux limit) is fitted by a relatively warm SED template and gives an $L_{IR} = 8.3^{+4.7}_{-4.4} \times 10^{11}\ L_\odot$ after correction for magnification. All of the IR SED templates give L_{IR} estimates less than $1.3 \times 10^{12}\ L_\odot$.
3. The IRS long-low spectra show strong PAH emission at 6.2 and 7.7 μm that dominate the mid-IR luminosity. The EWs are near the maximum observed in local starburst galaxies (Brandl et al. 2006; Desai et al. 2007; Imanishi et al. 2007) as well as high-redshift ULIRGs with strong PAH emission (Sajina et al. 2007; Pope et al. 2008). There are only small differences in the PAH flux ratios and overall spectral shape of the Cosmic Eye and composite spectra of local starbursts and high-redshift SMGs, as well as the lensed LBG, cB58. However, the $L_{7.7}/L_{6.2}$ PAH ratio of the SMG composite is significantly higher than that of both lensed LBGs. The Cosmic Eye lies along the L_{PAH}-to-L_{IR} correlations seen in starburst galaxies spanning 3 orders of magnitude in luminosity (Pope et al. 2008; Rigby et al. 2008; Menéndez-Delmestre et al. 2009). Confirming this correlation in LBGs is important, as many of the IR-derived SFRs are currently based on 24 μm fluxes alone, which are dominated by PAH emission.
4. In the IRS short-low spectrum, we detect the 3.3 μm PAH. This is the highest redshift detection of this line and only the second reported detection outside of the local universe ($z > 0.2$; Sajina et al. 2009). The PAH ratio, $L_{6.2}/L_{3.3} = 5.8 \pm 1.7$, is similar to the average ratio observed ($\sim$6) in local ULIRGs (Imanishi et al. 2006, 2007) and the 3.3-to-L_{IR} ratio, $L_{3.3}/L_{IR} = 8.5 \times 10^{-4}$, is consistent with measurements from local starbursts (Mouri et al. 1990; Imanishi 2002). This line is of particular interest as it is the only strong PAH feature accessible with *JWST* at $z > 3$ and may greatly facilitate studies of dust in the early universe. Further measurements (in other LBGs) of the 3.3 μm feature's relation to other PAHs and to L_{IR} are needed in order to interpret *JWST* measurements in the future.
5. Given an intrinsic UV spectral slope and a reddening curve, the observed spectral slope should predict the amount of IR emission (reprocessed UV light absorbed by dust) relative to unabsorbed UV light. The measured L_{FIR}/L_{UV} ratio is eight times lower than predicted from the UV spectral slope when assuming a Calzetti reddening curve. That is, the Eye lies significantly below the IRX–β relation measured in local starbursts (Meurer et al. 1999). This has also been observed in the only other LBG to have detailed *Spitzer* data, cB58 (Siana et al. 2008). Steeper extinction curves such as the LMC or SMC curves can rectify this apparent discrepancy. Siana et al. (2008) argue that the extinction curve is steeper than a Calzetti curve because much of the dust is in an outflowing foreground sheet with a large covering factor (near unity). The Cosmic Eye, as with cB58, exhibits opaque absorption lines from outflowing gas, indicative of a high covering fraction of outflowing dust. Therefore, we argue that both of these LBGs have steeper extinction curves than the Calzetti law due to dust geometries that differ from the patchy extinction seen in local starbursts. However, a different dust composition cannot be ruled out as a possible explanation for the discrepant reddening law.

I.R.S., K.E.K.C., and A.C.E. acknowledge support from STFC. A.M.S. also acknowledges support from the RAS Lockyer Fellowship. J.R. acknowledges support from an EU Marie Curie Fellowship.

This work is based on observations made with the *Spitzer Space Telescope*, which is operated by the Jet Propulsion Laboratory, California Institute of Technology under a contract with NASA. Support for this work was provided by NASA through an award issued by JPL/Caltech.

Facilities: Spitzer

REFERENCES

Adelberger, K. L., & Steidel, C. C. 2000, ApJ, 544, 218
Allam, S. S., Tucker, D. L., Lin, H., Diehl, H. T., Annis, J., Buckley-Geer, E. J., & Frieman, J. A. 2007, ApJ, 662, L51
Bell, E. F. 2002, ApJ, 577, 150
Belokurov, V., et al. 2007, ApJ, 671, L9
Bendo, G. J., et al. 2006a, ApJ, 645, 134
Bendo, G. J., et al. 2006b, ApJ, 652, 283
Brandl, B. R., et al. 2006, ApJ, 653, 1129
Bruzual, G. 2007, arXiv:astro-ph/0703052
Calzetti, D. 1997, AJ, 113, 162
Calzetti, D., Armus, L., Bohlin, R. C., Kinney, A. L., Koornneef, J., & Storchi-Bergmann, T. 2000, ApJ, 533, 682
Calzetti, D., Kinney, A. L., & Storchi-Bergmann, T. 1994, ApJ, 429, 582
Calzetti, D., et al. 2005, ApJ, 633, 871
Carilli, C. L., et al. 2008, ApJ, 689, 883
Chapman, S. C., Blain, A. W., Smail, I., & Ivison, R. J. 2005, ApJ, 622, 772
Chapman, S. C., et al. 2000, MNRAS, 319, 318
Chary, R., & Elbaz, D. 2001, ApJ, 556, 562
Coppin, K. E. K., et al. 2007, ApJ, 665, 936
Desai, V., et al. 2007, ApJ, 669, 810
Draine, B. T., & Li, A. 2007, ApJ, 657, 810
Dye, S., Smail, I., Swinbank, A. M., Ebeling, H., & Edge, A. C. 2007, MNRAS, 379, 308
Ellingson, E., Yee, H. K. C., Bechtold, J., & Elston, R. 1996, ApJ, 466, L71
Engelbracht, C. W., et al. 2006, ApJ, 642, L127
Erb, D. K., Steidel, C. C., Shapley, A. E., Pettini, M., Reddy, N. A., & Adelberger, K. L. 2006, ApJ, 647, 128
Fitzpatrick, E. L. 1986, AJ, 92, 1068
Frayer, D. T., et al. 2006, ApJ, 647, L9
Gil de Paz, A., et al. 2005, ApJ, 627, L29
Goldader, J. D., Meurer, G., Heckman, T. M., Seibert, M., Sanders, D. B., Calzetti, D., & Steidel, C. C. 2002, ApJ, 568, 651
Holwerda, B. W., Keel, W. C., Williams, B., Dalcanton, J. J., & de Jong, R. S. 2009, AJ, 137, 3000
Hummer, D. G., & Storey, P. J. 1987, MNRAS, 224, 801
Imanishi, M. 2002, ApJ, 569, 44
Imanishi, M., & Dudley, C. C. 2000, ApJ, 545, 701
Imanishi, M., Dudley, C. C., Maiolino, R., Maloney, P. R., Nakagawa, T., & Risaliti, G. 2007, ApJS, 171, 72
Imanishi, M., Dudley, C. C., & Maloney, P. R. 2006, ApJ, 637, 114
Imanishi, M., Nakagawa, T., Ohyama, Y., Shirahata, M., Wada, T., Onaka, T., & Oi, N. 2008, PASJ, 60, 489
Kennicutt, R. C. Jr., 1998, ARA&A, 36, 189
Latter, W. B. 1991, ApJ, 377, 187
Lin, H., et al. 2008, arXiv:0809.4475
Magnelli, B., Chary, R. R., Pope, A., Elbaz, D., Morrison, G., & Dickinson, M. 2008, ApJ, 681, 258
Maiolino, R., Schneider, R., Oliva, E., Bianchi, S., Ferrara, A., Mannucci, F., Pedani, M., & Roca Sogorb, M. 2004, Nature, 431, 533

Makovoz, D., & Khan, I. 2005, in ASP Conf. Ser. 347, Astronomical Data Analysis Software and Systems XIV, ed. P. Shopbell, M. Britton, & R. Ebert (San Francisco, CA: ASP), 81
Makovoz, D., & Marleau, F. R. 2005, PASP, 117, 1113
Menéndez-Delmestre, K., et al. 2009, arXiv:0903.4017
Meurer, G. R., Heckman, T. M., & Calzetti, D. 1999, ApJ, 521, 64
Moorwood, A. F. M. 1986, A&A, 166, 4
Mouri, H., Kawara, K., Taniguchi, Y., & Nishida, M. 1990, ApJ, 356, L39
Papovich, C., Dickinson, M., & Ferguson, H. C. 2001, ApJ, 559, 620
Pettini, M., & Pagel, B. E. J. 2004, MNRAS, 348, L59
Pettini, M., Steidel, C. C., Adelberger, K. L., Dickinson, M., & Giavalisco, M. 2000, ApJ, 528, 96
Pilyugin, L. S., & Thuan, T. X. 2005, ApJ, 631, 231
Pope, A., et al. 2008, ApJ, 675, 1171
Prevot, M. L., Lequeux, J., Prevot, L., Maurice, E., & Rocca-Volmerange, B. 1984, A&A, 132, 389
Reddy, N. A., & Steidel, C. C. 2004, ApJ, 603, L13
Reddy, N. A., & Steidel, C. C. 2009, ApJ, 692, 778
Reddy, N. A., Steidel, C. C., Fadda, D., Yan, L., Pettini, M., Shapley, A. E., Erb, D. K., & Adelberger, K. L. 2006, ApJ, 644, 792
Rigby, J. R., et al. 2008, ApJ, 675, 262
Risaliti, G., et al. 2006, MNRAS, 365, 303
Sajina, A., Yan, L., Armus, L., Choi, P., Fadda, D., Helou, G., & Spoon, H. 2007, ApJ, 664, 713
Sajina, A., Yan, L., Spoon, H., & Fadda, D. 2009, arXiv:0901.4284
Shapley, A. E., Steidel, C. C., Adelberger, K. L., Dickinson, M., Giavalisco, M., & Pettini, M. 2001, ApJ, 562, 95
Siana, B., Teplitz, H. I., Chary, R.-R., Colbert, J., & Frayer, D. T. 2008, ApJ, 689, 59
Smail, I., et al. 2007, ApJ, 654, L33
Stark, D. P., Swinbank, A. M., Ellis, R. S., Dye, S., Smail, I. R., & Richard, J. 2008, Nature, 455, 775
Steidel, C. C., Giavalisco, M., Pettini, M., Dickinson, M., & Adelberger, K. L. 1996, ApJ, 462, L17
Stratta, G., Maiolino, R., Fiore, F., & D'Elia, V. 2007, ApJ, 661, L9
Teplitz, H. I., et al. 2000, ApJ, 533, L65
Teplitz, H. I., et al. 2007, ApJ, 659, 941
Thilker, D. A., et al. 2005, ApJ, 619, L79
Tielens, A. G. G. M. 2008, ARA&A, 46, 289
Todini, P., & Ferrara, A. 2001, MNRAS, 325, 726